Article No. jmbi.1998.2441 available online at http://www.idealibrary.com on IDEAL J. Mol. Biol. (1999) 285, 1903–1909

JMB

COMMUNICATION

Surface Structures of Native Bacteriorhodopsin Depend on the Molecular Packing Arrangement in the Membrane

Daniel J. Müller[1]*, Hans-Jürgen Sass[2], Shirley A. Müller[1], Georg Büldt[2] and Andreas Engel[1]

[1]*M. E. Müller-Institute for Microscopic Structural Biology Biozentrum University of Basel Klingelbergstrasse 70 CH-4056 Basel, Switzerland*

[2]*Forschungszentrum Jülich IBI-2: Structural Biology D-52425 Jülich, Germany*

**Corresponding author*

Bacteriorhodopsin is the one of the best-studied models of an ion pump. Five atomic models are now available, yet their comparison reveals differences of some loops connecting the seven transmembrane α-helices. In an attempt to resolve this enigma, topographs were recorded in aqueous solution with the atomic force microscope (AFM) to reveal the most native surface structure of bacteriorhodopsin molecules in the purple membrane. Individual peptide loops were observed with a lateral resolution of between 4.5 Å and 5.8 Å, and a vertical resolution of about 1 Å. The AFM images demonstrate for the first time, that the shape, the position, and the flexibility of individual polypeptide loops depend on the packing arrangement of bacteriorhodopsin molecules in the lipid bilayer.

Keywords: bacteriorhodopsin; purple membranes; atomic force microscopy

Bacteriorhodopsin (BR), a light-driven proton pump (Oesterhelt & Stoeckenius, 1973), is packed into highly ordered trigonal two-dimensional (2D) lattices (Henderson, 1975) to form the purple membrane of *Halobacterium salinarum*. Electron crystallography of these membranes produced the first three-dimensional (3D) structure of a membrane protein (Henderson & Unwin, 1975), and finally the first atomic model of BR (Henderson *et al.*, 1990; Grigorieff *et al.*, 1996). The loops connecting the α-helices A and B, B and C, and E and F appeared to be disordered as they could not be resolved reliably. Progress in instrumentation and the improved structural preservation obtained by trehalose embedding and rapid-freezing techniques (Henderson *et al.*, 1990) have made it possible to collect electron microscopy data to a resolution of 3 Å (Kimura *et al.*, 1997). As a result, most loops have now been resolved as clearly as the α-helical transmembrane regions. 3D BR crystals grown in a cubic lipid phase (Landau & Rosenbusch, 1996) have recently allowed the structure of BR to be determined to a resolution of 2.5 Å (Pebay-Peyroula *et al.*, 1997) and 2.3 Å (Luecke *et al.*, 1998) by X-ray crystallography. Furthermore, heterogeneous nucleation of BR trimers into 3D crystals allowed preservation of the purple membrane lipid composition and the structural determination of the bacteriorhodopsin-lipid complex to 2.9 Å (Essen *et al.*, 1998). The atomic models correlate well in the α-helical regions, but differ significantly in their surface structures. In the X-ray maps of BR crystals grown in a cubic lipid phase, some of the peptide loops were visualized clearly, while others appeared to be disordered. This suggests that the experimental methods employed to solve the BR structure influenced the structure of the hydrophilic loops at the BR surfaces. Hence it would be meaningful to image BR in its most native state (Sass *et al.*, 1997), namely in the membrane and in buffer solution.

Here, we compare atomic force microscopy (AFM) topographs of BR in native purple membranes (Müller *et al.*, 1995a,b, 1996) and of BR assembled *in vitro* into an orthorhombic lattice (Michel *et al.*, 1980). All topographs were recorded in the same buffer solution (100 mm KCl, 10 mM

Abbreviations used: AFM, atomic force microscopy; BR, bacteriorhodopsin; RMS, root-mean-square; SD, standard deviation; 2D, two-dimensional; 3D, three-dimensional.

E-mail address of the corresponding author: muellerda@ubaclu.unibas.ch

0022-2836/99/051903–07 $30.00/0

Tris(pH 7.8), and under identical scan conditions, except that different forces were applied to the stylus.

High-resolution topographs were acquired in buffer solution

The cytoplasmic BR surface imaged with a force of 100 pN applied to the AFM stylus revealed trimeric structures arranged in a trigonal lattice of 62(±2) Å side length (Figure 1(a)). Subunits in the trimer featured a particularly pronounced protrusion extending 8.3(±1.9) Å ($n = 398$) above the lipid surface. As shown previously, this protrusion arises from the loop connecting transmembrane α-helices E and F (Müller *et al.*, 1995b). The power spectrum of the topograph included 11th-order diffraction spots (Figure 1(b)) demonstrating that a lateral resolution of 4.9 Å has been achieved.

At applied forces above 200 pN, AFM topographs were significantly different. The prominent E-F loops were bent away and the shorter loops of the BR monomers were visualized (Figure 1(c)). This conformational change is fully reversible (Müller *et al.*, 1995b), suggesting that loop E-F is a rather flexible element on the cytoplasmic side of the BR molecule. At this force of 200 pN, the maximum height difference between the protein and the lipid membrane was 6.4(±1.2) Å ($n = 398$). Three distinct protrusions were recognized in almost every monomer, and a further distinct protrusion was present at the center of the trimers. The calculated diffraction pattern (Figure 1(d)) documents an isotropic resolution out to 4.5 Å.

Topographs of the native extracellular BR surface acquired with the AFM using an applied force of 100 pN revealed the arrangement of tripartite protrusions on a trigonal lattice (Figure 1(e)). The maximum height difference between the protein and the lipid membrane was 5.3(±0.7) Å ($n = 320$). The power spectrum (Figure 1(f)) exhibited characteristic strong second-order spots, and extended to

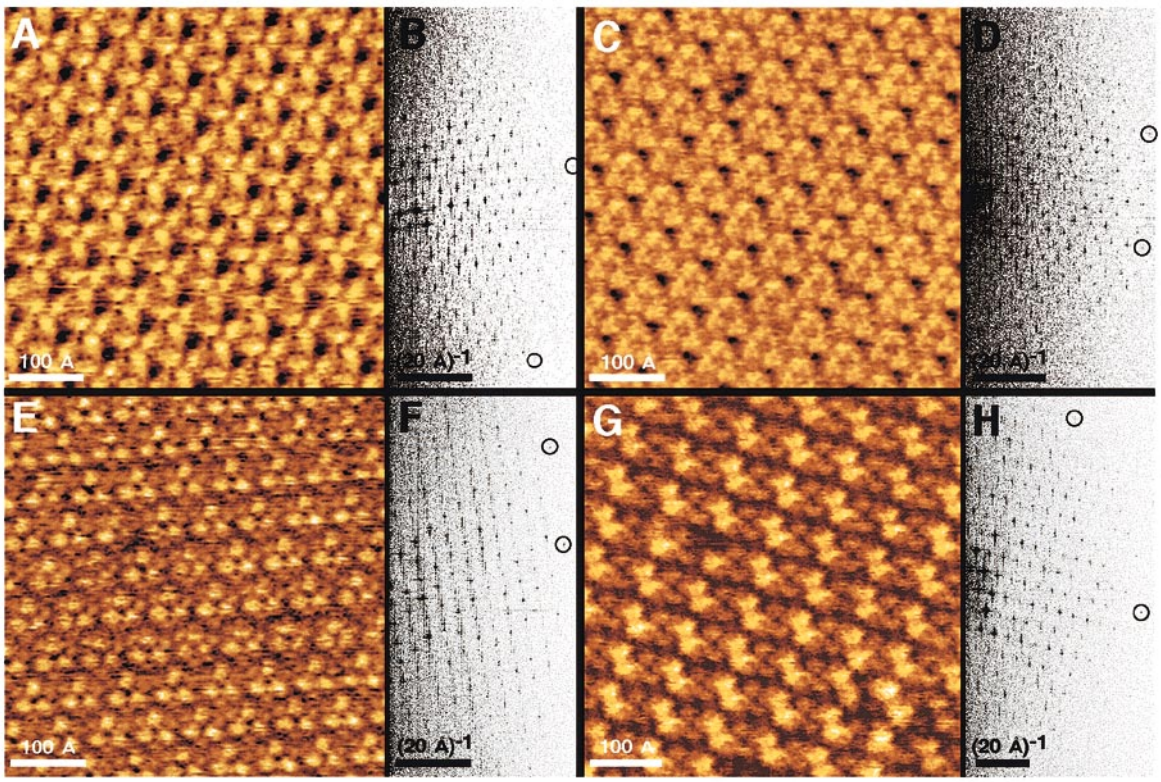

Figure 1. Purple membrane surfaces as observed in buffer solution using the AFM. (a) Native cytoplasmic surface recorded at 100 pN. (b) Power spectrum of (a). (c) Cytoplasmic surface recorded at 200 pN. (d). Power spectrum of (c). (e) Native extracellular surface recorded at 100 pN. (f) Power spectrum of (e). (g) Orthorhombic crystal of BR recorded at 100 pN. In this crystal form ($p22_12_1$) the rows of BR dimers alternate, to expose either their cytoplasmic or their extracellular surfaces to the aqueous solution. (h) Power spectrum of (g). Vertical brightness range of topographs: 10 Å. Purple membranes were isolated from *Halobacterium salinarum* (ET1001) (Oesterhelt & Stoeckenius, 1974) and orthorhombic 2D crystals were prepared as described (Michel *et al.*, 1980). In all cases, the samples were adsorbed onto freshly cleaved mica in buffer solution (300 mM KCl, 10 mM Tris-HCl (pH 7.8); Müller *et al.*, 1997), while the buffer solution used for recording the high-resolution topographs was 100 mM KCl, 10 mm Tris-HCl (pH 7.8). The atomic force microscope used was a Nanoscope III (Digital Instruments, Santa Barbara, California) equipped with an E-scanner (12 μm) and oxide sharpened Si_3N_4 tips on a cantilever with a spring constant of 0.1 N/m (Olympus, Tokyo, Japan). Topographs recorded in trace and retrace scanning directions using contact mode showed no significant differences. All measurements were carried out at room temperature.

the 11th order indicating a lateral resolution of 4.9 Å. In contrast to the cytoplasmic surface, increasing the force applied to the stylus did not cause structural changes in the individual extracellular loops. However, in these images it is difficult to assign the center of the BR trimer unambiguously (Müller *et al.*, 1996). For this reason, we also investigated *in vitro* reassembled membranes of a dimeric form of BR.

Recrystallization of BR in the presence of *n*-dodecyl trimethylammonium chloride (DTAC) yielded well-ordered 2D crystals (Michel *et al* 1980) that adsorbed flatly onto freshly cleaved mica. They had sizes of up to 5 μm, and a thickness of 58(±4) Å ($n = 113$), which was slightly more than that of the native purple membrane 55(±4) Å (Müller & Engel, 1997). As expected, topographs of the orthorhombic crystal showed BR dimers assembled into a rectangular lattice with a $p22_12_1$ symmetry and unit cell dimensions of $a = 58$ Å, $b = 74$ Å (Figure 1(g)); Michel *et al.*, 1980). Accordingly, the BR dimers alternately had their cytoplasmic surface or their extracellular surface facing the stylus. The maximum height difference between the protrusions and the bilayer was 8.1(±0.9) Å ($n = 368$). The power spectrum revealed diffraction spots to the tenth order indicating a resolution of 5.8 Å (Figure 1(h)). Surprisingly, it was not possible to induce conformational changes of the E-F loops in this BR crystal form. Increasing the applied force of the stylus resulted in a deformation of the whole protein surface rather than in the bending of a single loop, and reduced the lateral resolution.

A striking feature of all unprocessed topographs displayed in Figure 1 is their high signal-to-noise ratio. Smallest details are not only resolved laterally, but their height is highly reproducible as revealed by comparing different unit cells and considering that the full gray level range represents 10 Å.

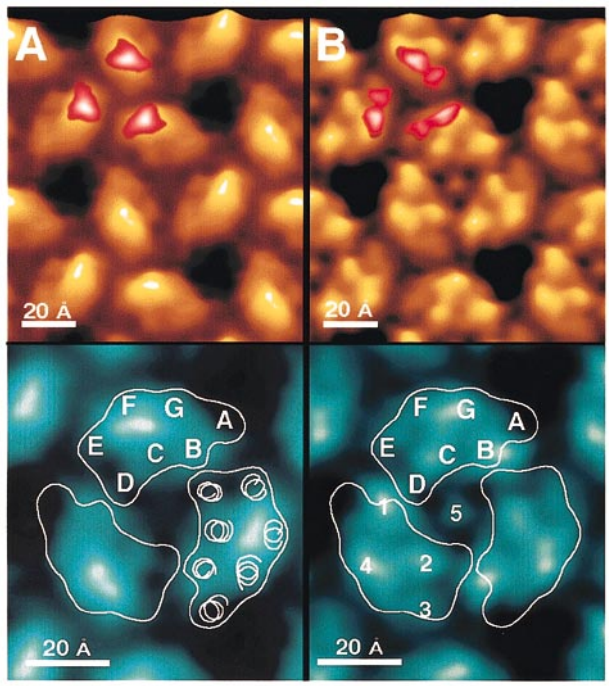

Figure 2. Averaged cytoplasmic surface of the BR trimer of purple membrane. (a) Native cytoplasmic surface recorded at applied forces of 100 pN (average of 398 unit cells). (b) Native cytoplasmic surface recorded at applied forces of 200 pN (average of 380 unit cells). Correlation averages are displayed in perspective view (top, shaded in yellow-brown) and in top view (bottom, in blue) with full brightness ranges of 10 Å. To assess the flexibility of the different structures, standard deviation (SD) maps were calculated (Karrasch *et al.*, 1994; Müller *et al.*, 1998), and had a range from 0.8 (lipid) to 1.9 Å (extended E-F loop; see Table 1). Surface regions exhibiting a SD above 1.2 Å are superimposed in red-to-white shades. The outlined BR shapes were adapted from sections close to the cytoplasmic surface of BR trimers obtained from electron crystallographic analyses (Figure 3; Grigorieff *et al.*, 1996). The correlation-averaged topographs were 3-fold symmetrized and exhibited 9.2% (a), and 14.1% (b) root-mean-square (RMS) deviation from *P*3 symmetry.

Averaged AFM topographs reveal structural changes on the cytoplasmic surface of BR

Imaged in its most extended form the E-F loop of bacteriorhodopsin from the native purple membrane reached its maximum height above the lipid bilayer of 8.3 Å close to helix F (Figure 2(a)). While the standard deviation (SD) of the height measurements was around 1 Å for most morphological features of the topography, the E-F loop exhibited a SD of 1.9 Å (Table 1), consistent with the high temperature factor observed by electron microscopy (Grigorieff *et al.*, 1996). The height of 8.3 Å correlates well with the 3D maps from electron crystallographic analyses (Figure 3) which showed helix F to protrude out of the bilayer by 7 to 10 Å, whereas helix E either did not extend into the aqueous phase (Kimura *et al.*, 1997), or protruded only slightly above the bilayer (Figure 3(a); Grigorieff *et al.*, 1996)). However, in the X-ray structure by Essen *et al.* (1998) helix E protrudes out of the bilayer by approximately 5 Å. Nevertheless, helix F represents the highest protrusion at the cytoplasmic surface in this structure as well. Two minor protrusions in the AFM topograph are localized close to helix B and between helices C and D, respectively. When the major protrusion representing loop E-F had been pushed away by applying a force of 200 pN to the stylus, the cytoplasmic surface of the BR molecule appeared different and exhibited finer details (Figure 2(b)). The protrusion between helices F and G (no. 4) together with the minor elevation close to helix E (no. 3) is likely to represent what remained from loop E-F and the protruding parts of helices E and F that are compressed by the AFM stylus. However, it cannot be excluded that the protrusion between helices F and G represents part of the 25 amino acid residue long

Table 1. Heights (in Å) of protrusions in the trigonal and orthorhombic crystals

Heights (Å) ± SD of:	Trigonal crystal	Orthorhombic crystal
Membrane	55 ± 4	58 ± 4
Cytoplasmic surface:	($n = 398$)	($n = 368$)
Extended E-F loop	8.3 ± 1.9	-
Protrusion 1	5.8 ± 0.8	4.5 ± 0.9
Protrusion 2	5.6 ± 0.7	6.8 ± 0.9
Protrusion 3	4.2 ± 1.1	6.8 ± 0.9
Protrusion 4	6.4 ± 1.2	8.1 ± 0.9
Protrusion 5	3.6 ± 0.9	3.9 ± 0 9
Protrusion 6	-	7.6 ± 0.9
Extracellular surface:	($n = 320$)	($n = 368$)
Protrusion 7	3.3 ± 1.2	2.2 ± 0.7
Protrusion 8	2.7 ± 0.7	4.0 ± 0.8
Protrusion 9	5.3 ± 0.7	3.8 ± 0.9
Protrusion 10	-	2.8 ± 0.6
Protrusion 11	3.3 ± 0.7	-
Protrusion 12	0.8 ± 0.7	-
Protrusion 13	1.4 ± 0.7	-

The numbers of protrusions refer to protrusions defined in the averaged topographs (Figures 2 and 4). Vertical distances are given relative to the surface of the lipid bilayer, except for the membrane thicknesses which were measured relative to the support and in the absence of repulsive electrostatic double-layer interactions (Müller & Engel, 1997). The standard deviations (SD) of the averaged topographs were calculated during the averaging of the unit cells. The number of unit cells averaged is represented by n

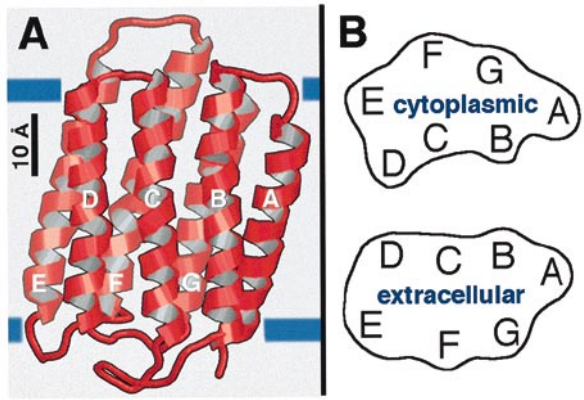

Figure 3. Structure of bacteriorhodopsin. (a) Ribbon representation as revealed by electron crystallography (Grigorieff *et al*., 1996). Because of their disordering, the N terminus of helix A and the C terminus of helix G were not resolved and the B-C loop was only partly resolved. Blue lines indicate the cytoplasmic and extracellular surfaces determined by Kimura *et al*. (1997). (b) Outlines of 10 Å thick slices of the cytoplasmic and the extracellular BR surface. (Data were kindly provided by N. Grigorieff and R. Henderson (Grigorieff *et al*., 1996).)

C-terminal domain. This uncertainty arises because the AFM height signal in this area exhibited a significant standard deviation (red shaded in Figure 2(b) and see Table 1), consistent with the elevated temperature factor of this region determined by electron microscopy (Grigorieff *et al*., 1996). The other protrusions in the AFM topograph may be assigned by comparison with the atomic models derived from the BR trimer (Grigorieff *et al*., 1996; Kimura *et al*., 1997; Essen *et al*., 1998). In these models helix B protrudes out of the bilayer, and helix A ends below the bilayer surface (Figure 3(a)). Therefore, the topographic protrusion no. 1 is likely to represent the short loop (seven amino acid residues) connecting helices A and B (Figure 2(b)). In addition, the discrete protrusion between helices C and D (no. 2) correlates to their connecting loop (three amino acid residues). A further protrusion (no. 5) of 2 Å height was present at the 3-fold axis of the BR trimer and probably arises from lipid molecules (Grigorieff *et al*., 1996).

The arrangement of the protrusions on the cytoplasmic face of BR was very distinct when AFM topographs of the orthorhombic *in vitro* assemblies were analysed. The protrusion of the A-B loop (no. 1) was shifted by 3 Å, now being located between the position of helices A and B (Figure 4(a)). The short loop (three amino acid residues) connecting helices C and D was observed as a discrete protrusion (no. 2) in the orthorhombic lattice, close to its position in the trigonal lattice. Remarkably, the E-F loop was observed as a bean-shaped structure independent of the applied force (Figure 4(a); protrusions no. 3 and no. 6). The triangular protrusion (no. 4) located between helices B and G may result from the C terminus. None of these structures exhibited significant variabilities, indicating a structural stabilization by the different packing arrangement in the orthorhombic compared to the trigonal lattice. An additional protrusion (Figure 4(a), no. 5) was observed at the periphery of each BR monomer packed in the orthorhombic lattice, probably representing bound lipid molecules (Grigorieff *et al*., 1996).

The observed structural changes suggest that the interactions of the cytoplasmic polypeptide loops depend on how the BR molecules associate. In the BR trimer, there is a crevice between helices A and B, and helices E and D of neighboring monomers (Figure 2; outlines). Lipid molecules in this crevice arestable (Grigorieff *et al*., 1996), and stabilize the BR trimer by specific interactions with their lipid and head-group moieties (Essen *et al*., 1998). This crevice is not present in the orthorhombic BR assembly and hence, the different molecular interactions probably allow the displacement of the loop connecting helices A and B (Figure 4(a); white contours). Helices F and G of two neighboring BR molecules are closely packed providing space for at most two lipid molecules. Consistent with the stability of the E-F loops the standard deviation over this region was not enhanced as in the trigonal crystal (Table 1). Differences in helix E have also been observed in X-ray structures from different crystal forms. While the end of helix E has not been resolved in the crystals grown in the cubic lipid phase (Pebay-Peyroula *et al*., 1997; Luecke

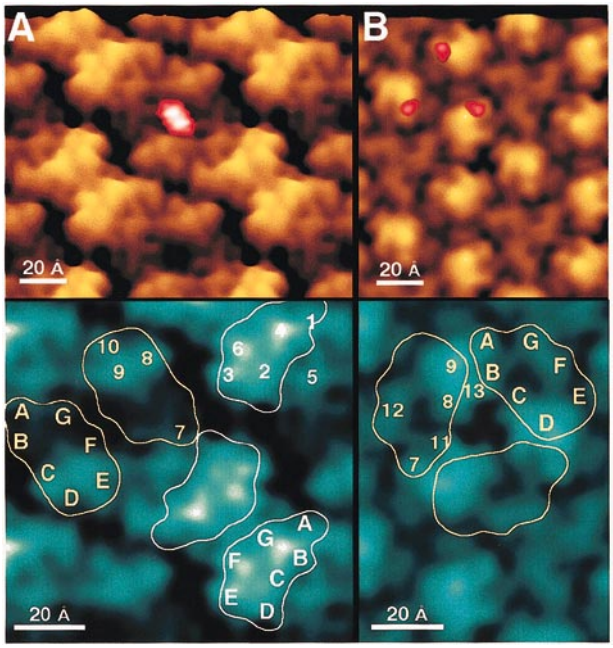

Figure 4. Averaged surface of BR assembled into an orthorhombic lattice (a) and of the extracellular surface of purple membrane (b) Correlation averages (average of 368 unit cells (a) and of 320 unit cells (b)) were displayed in perspective view (top, shaded in yellow-brown) and in top view (bottom, shaded in blue) with a vertical brightness range of 10 Å. The SD map had a range from 0.7 (lipid) to 1.7 Å (F-G region). Surface regions exhibiting a SD above 1.2 Å are superimposed in red-to-white shades (see Table 1). The correlation-averaged topograph of the orthorhombic lattice (a) was 2-fold symmetrized exhibiting a 2.1% RMS deviation from *P*2 symmetry, whereas the 3-fold symmetrized extracellular surface (b) exhibited an 6.1% RMS deviation from *P*3 symmetry. Topographs were recorded at applied forces of 100 pN. The outlined sections were adapted from electron crystallographic analyses. Based on the projection map of orthorhombic BR crystals (Michel *et al.*, 1980; Leifer & Henderson, 1983), cytoplasmic and extracellular sections of the BR molecule revealed from trigonal crystals (Grigorieff *et al.*, 1996) were arranged on the orthorhombic lattice. With the knowledge of the extracellular protrusions on the orthorhombic crystal (Figure 4(a)), it was possible to align the averaged AFM topographs of the extracellular bacteriorhodopsin surface (Figure 4(b)) with the extracellular section of the BR trimers obtained from electron crystallography (Figure 3(b)); Grigorieff *et al.*, 1996).

et al., 1998), helix E was stable and fully resolved in the structure by Essen *et al.* (1998), where crystal contacts along helices F and G occur. Accordingly, we conclude that in the orthorhombic BR crystals the interactions between helices F and G of two adjacent BR molecules affected both the structural appearance and the rigidity of the E-F loop and of the C-terminal region. In addition, the protrusion of loop A-B was shifted towards helix A in the orthorhombic lattice, away from the intermolecular space.

Extracellular surface features differ between BR crystal forms

The extracellular surface of BR assembled into an orthorhombic lattice (Figure 4(a); yellow outline) exhibited distinct features which were correlated to the atomic model. Protrusion no. 7 of the monomer was located close to helix A and may also represent part of the N-terminal domain (seven amino acid residues). Whereas no protrusion was observed at the position of helix B, protrusions no. 8 and no. 9 correlate with the β-hairpin connecting helices B and C (Kimura *et al.*, 1997; Essen *et al.*, 1998). The short loop connecting helices E and D appears to be represented by protrusion no. 10. The region between helices F and G exhibited an enhanced standard deviation (1.7 Å; Figure 4(a); red colored) and the connecting loop did not make a structural contribution to the average. Thus, in contrast to the cytoplasmic surface, the crystal contacts along helices F and G did not stabilize the corresponding extracellular loops.

On the extracellular surface of native purple membrane (Figure 4(b), protrusion no. 7 arising from the N-terminal region is at the same position in the BR trimer as in the orthorhombic crystal. In contrast to the latter, a small protrusion (no. 11) is observed at the location of helix B. The β-hairpin (Kimura *et al.*, 1997; Essen *et al.*, 1998), represented by protrusions no. 8 and no. 9, starts at helix B, propagates back into the lipid bilayer to create a depression seen between protrusion no. 11 and no. 8. Compared to the topography of the orthorhombic crystal, protrusion no. 9 is shifted by 11 Å away from the center of the BR molecule and its height above the bilayer is increased by 1 Å. The rather large rearrangement of the B-C loop observed in the orthorhombic lattice presumably results from the different crystal contacts and the altered proteinaceous and lipidic interactions. Similarly, the loop connecting helices F and G, which is mobile in the orthorhombic lattice, was observed as a stable protrusion (no. 12) in the BR trimer and exhibited no significant standard deviation. Protrusion no. 13 (Figure 4(b)) was observed at the position of the triglycoside head-groups of lipids which were found to occur ordered in the crevice between two BR monomers (Essen *et al.*, 1998). In addition, the topograph of native purple membrane shows a depression at the center of the extracellular side of the BR molecule (Figure 4(b), where protons are assumed to exit the protein.

Conclusions

As demonstrated by comparing the atomic models of BR presented by Grigorieff *et al.* (1996), Kimura *et al.* (1997), Pebay-Peyroula *et al.* (1997), Essen *et al.* (1998) and Luecke *et al.* (1998), structures which are shielded by the hydrophobic belt

of the bilayer are not greatly influenced by the preparation technique. This is in contrast to structures that face the aqueous solution. The presented AFM topographs of two BR crystal forms clearly show differences in structural detail reflecting the shifting of loops of the BR molecule. Interestingly, the flexibility of some of the loops was also influenced. Since the sensitivity (2) of the AFM is sufficient to image individual loops in their extended conformation (Mü1ler *et al*., 1995b), the deformations induced by the imaging process at forces of <100 pN can be neglected. However, it was possible to force loop E-F of the BR trimer to undergo a conformational change of about 2 Å by increasing the force applied to the AFM cantilever >200 pN, which corresponds to an energy difference of 4 kJ/mol. Our experimental results, therefore, demonstrate for the first time that the shape, the position, and the flexibility of individual polypeptide loops exposed to the aqueous solution depend on the packing arrangement of proteins within the lipid bilayer.

Although such structural changes may not significantly influence the proton pumping function of bacteriorhodopsin (Michel *et al*., 1980), they may influence the pathway of protons on the protein surface (Heberle *et al*., 1994), a topic which is presently discussed on the basis of static models (Kimura *et al*., 1997; Essen *et al*., 1998; Luecke *et al*., 1998). Bacteriorhodopsin, one of the best-characterized transmembrane proteins, exhibits structural homologies to the seven-helix G-protein-coupled receptor family (Hargrave, 1991; Baldwin, 1993). The observed structural changes may be of crucial importance for these membrane proteins whose surface regions are known to interact with other proteins.

Acknowledgments

We thank Jacques Dubochet, Joerg Kistler, Ehud Landau, and Jurg Rosenbusch for critical reading of the manuscript. This work was supported by the Swiss National Foundation for Scientific Research, grant 31-424335.94 to A.E., and the Maurice E. Müller Foundation of Switzerland.

References

Baldwin, J. M. (1993). The probable arrangement of the helices in G protein-coupled receptors. *EMBO J.* **12**, 1693-1703.

Essen, L.-O., Siegert, R., Lelimann, W. D. & Oesterhelt, D. (1998). Lipid patches in membrane protein oligomers: Crystal structure of the bacteriorhodopsin-lipid complex. *Proc. Natl Acad. Sci. USA,* **95**, 11673-11678.

Grigorieff, N., Ceska, T. A., Downing, K. H., Baldwin, J. M. & Henderson, R. (1996). Electron-crystallographic refinement of the structure of bacteriorhodopsin. *J. Mol. Biol.* **259**, 393-421.

Hargrave, P. A. (1991). Seven-helix receptors. *Curr. Opin. Struct. Biol.* **1**, 575-581.

Heberle, L., Riesle, L., Thiedemann, G., Oesterhelt, D. & Dencher, N. A. (1994). Proton migration along the membrane surface and retarded surface to bulk transfer. *Nature,* **370**, 379-382.

Henderson, R. (1975). The structure of the purple membrane from *Halobacterium halobium*: analysis of the X-ray diffraction pattern. *J. Mol. Biol.* **93**, 123-138.

Henderson, R. & Unwin, P. N. T. (1975). Three-dimensional model of purple membrane obtained by electron microscopy. *Nature,* **257**, 28-32.

Henderson, R., Baldwin, J. M., Ceska, T. A., Zemlin, F., Beckman, E. & Downing, K. H. (1990). Model for the structure of bacteriorhodopsin based on high-resolution electron cryo-microscopy. *J. Mol. Biol.* **213**, 899-929.

Karrasch, S., Hegerl, R., Hoh, J., Baumeister, W. & Engel, A. (1994). Atomic force microscopy produces faithful high-resolution images of protein surfaces in an aqueous environment. *Proc. Natl Acad. Sci. USA,* **91**, 836-838.

Kimura, Y., Vassylev, D. G., Miyazawa, A., Kidera, A., Matsushima, M., Mitsuoka, K., Murata, K., Hirai, T. & Fujiyoshi, Y. (1997). Surface of bacteriorhodopsin revealed by high-resolution electron microscopy. *Nature,* **389**, 206-211.

Landau, E. M. & Rosenbusch, J. P. (1996). Lipidic cubic phases: a novel concept for the crystallization of membrane proteins. *Proc. Natl Acad. Sci. USA,* **93**, 14532-14535.

Leifer, D. & Henderson, R. (1983). Three-dimensional structure of orthorhombic purple membrane at 6.5 Å resolution. *J. Mol. Biol.* **163**, 451-466.

Luecke, H., Richter, H.-T. & Lanyi, J. K. (1998). Proton transfer pathways in bacteriorhodopsin at 2.3 Ångstrom resolution. *Science,* **80**, 1934-1937.

Michel, H., Oesterhelt, D. & Henderson, R. (1980). Orthorhombic two-dimensional crystal form of purple membrane. *Proc. Natl Acad. Sci. USA,* **77**, 338-342.

Müller, D. J. & Engel, A. (1997). The height of biomolecules measured with the atomic force microscope depends on electrostatic interactions. *Biophys. J.* **73**, 633-1644.

Müller, D. J., Schabert, F. A., Büldt, G. & Engel, A. (1995a). Imaging purple membranes in aqueous solutions at subnanometer resolution by atomic force microscopy. *Biophys. J.* **68**, 1681-1686.

Müller, D. J., Büldt, G. & Engel, A. (1995b). Force-induced conformational change of bacteriorhodopsin. *J. Mol. Biol.* **249**, 239-243.

Müller, D. J., Schoenenberger, C. A., Büildt, G. & Engel, A. (1996). Immuno-atomic force microscopy of purple membrane. *Biophys. J.* **70**, 1796-1802.

Müller, D. J., Amrein, M. & Engel, A. (1997). Adsorption of biological molecules to a solid support for scanning probe microscopy. *J. Struct. Biol.* **119**, 172-188.

Müller, D. L., Fotiadis, D. & Engel, A. (1998). Mapping flexible protein domains at subnanometer resolution with the AFM. *FEBS Letters,* **430**, 105-111.

Oesterhelt, D. & Stoeckenius, W. (1973). Functions of a new photoreceptor membrane. *Proc. Natl Acad. Sci. USA,* **70**, 2853-2857.

Oesterhelt, D. & Stoeckenius, W. (1974). Isolation of the cell membrane of *Halobacterium halobium* and its fraction into red and purple membrane. *Methods Enzymol.* **31**, 667-678.

Pebay-Peyroula, E., Rummel, G., Rosenbusch, J. P. & Landau, E. M. (1997). X-ray structure of bacteriorhodopsin at 2.5 Ångstroms from microcrystals grown in lipidic cubic phases. *Science,* **277**, 1676-1681.

Sass, H. J., Schachowa, I. W., Rapp, G., Koch, M. H. J., Oesterhelt, D., Dencher, N. A. & Büldt, G. (1997). The tertiary structural changes in bacteriorhodopsin occur between M states: X-ray diffraction and Fourier transform infrared spectroscopy. *EMBO J.* **16**, 1484-1491.

Edited by W. Baumeister

(Received 20 August 1998; received in revised form 18 November 1998; accepted 20 November 1998)